A Protocol to Characterize pH Sensing Materials and Systems

Mohamed T. Ghoneim, Atieh Sadraei, Pedro de Souza, Grace C. Moore, Martin Z. Bazant, and Canan Dagdeviren*

Although significant progress is made in identifying pH sensing materials and device configurations, a standard protocol for benchmarking performance of next-generation pH devices is still lacking. In particular, key properties of characterization systems, such as inherent component contributions, time plots for extended-gate field-effect transistor (EGFET) measurements, and the input resistance (R_{in}), often go unreported in studies of pH sensing systems. These properties strongly influence the characterization system and can lead to mistaken attribution of properties to the device. In this paper, a series of essential characterization tests and parameters are reported to evaluate pH systems, such as the zinc oxide EGFET, in a standardized protocol. This EGFET ZnO sensor has a sensitivity of −58.1 mV pH^{-1}, drift range from 2.5 to 14.2 µA h^{-1}, and response time of 136 s. By using a ZnO sensing electrode, it is demonstrated that i) intrinsic contributions of reference electrode and commercial transistor (for EGFET) are not negligible; ii) time plots for EGFET configuration and defining a critical point at the onset of drift are essential for accurate sensitivity, response time, and drift reporting; and iii) the results of the pH sensing system are strongly dependent on the input resistance of the used characterization instruments.

1. Introduction

Acidity sensing technology has advanced significantly since Walther Nernst's seminal postulate in 1889, relating ion concentrations to equilibrium electrode potential.[1] Soon after, Max Cremer observed the electric potential difference across a glass membrane separating solutions of different acidity or alkalinity, arising due to a nonequilibrium junction potential.[2–4] Soren Sorenson introduced the term "pH" in 1909[1] to denote the negative base-10 logarithm of the hydrogen ion concentration in aqueous solution, although this has been replaced by the hydrogen ion activity for thermodynamic consistency.[5] Many significant developments followed to measure the pH, mainly improving upon the glass electrode design and composition.[3] In modern times, alternate pH sensing methods have been considered in order to improve reliability and miniaturization. In the 1970s, Bergveld invented the ion-sensitive field-effect transistor (ISFET),[6] and Yates et al. introduced the site binding model for determining the surface potential due to adsorbed ions, which, in turn, influences the number of charge carriers and thus the drain to source current of the metal-oxide-semiconductor field-effect transistor (MOSFET).[7] van der Spiegel et al. developed the extended gate field-effect transistor (EGFET) using a depletion mode nMOS and iridium oxide (IrO$_x$) as multispecies microprobe, in 1983.[8] Today, traditional EGFET setups rely on a commercial enhancement mode transistor with its gate connected to the sensing electrode, made of an electrically conductive layer coated with pH-sensitive membrane. The accumulated charges at the sensing electrode affect the gate voltage of the transistor and modulate the channel current. The EGFET is a promising configuration for pH sensing systems that isolate the electronics from the electrochemical sensing electrode. These key developments paved the way for current research and opened new routes for investigations of materials and configurations for pH sensing systems.

A wide variety of materials have been investigated for their pH sensing capabilities, including metal oxides,[9–12] polymers,[13–18] and various nanostructures.[9,19–21] Many pH sensing systems have targeted biomedical applications,[22–25] such as monitoring healing wounds' pH,[13] and monitoring of pH for a heart undergoing ischemia.[11] Particularly, ZnO presents a useful model system because of its current use in multiple areas of research (i.e., as thin-film channel material, pH sensing membrane, and piezoelectric film), biocompatibility and ability to form various nanostructures. In 2005, the first application of ZnO membrane in EGFET setup was reported by Batista and Mulato using a commercial enhancement mode nMOS device and a reference electrode.[26]

Dr. M. T. Ghoneim, A. Sadraei, Prof. C. Dagdeviren
MIT Media Lab
Massachusetts Institute of Technology (MIT)
Cambridge, MA 02139, USA
E-mail: canand@media.mit.edu
P. de Souza, Prof. M. Z. Bazant
Department of Chemical Engineering
MIT
Cambridge, MA 02139, USA
Prof. M. Z. Bazant
Department of Mathematics
MIT
Cambridge, MA 02139, USA
G. C. Moore
Department of Materials Science and Engineering
MIT
Cambridge, MA 02139, USA

The ORCID identification number(s) for the author(s) of this article can be found under https://doi.org/10.1002/smtd.201800265.

**ADVANCED
SCIENCE NEWS**

www.advancedsciencenews.com

**small
methods**

www.small-methods.com

Recently, Ali introduced the interdigitated ZnO with nickel contacts EGFET, eliminating the need for the bulky reference electrode.[27] In addition, many recent reports focused on ZnO pH sensors in EGFET and ISFET configurations,[26,28–30] nanotube and nanorod structures,[20,31,32] as well as more traditional open-circuit potential (OCP) measurements.[22] However, essential information for reproducibility of pH measurements has not always been reported. The experimental results are therefore hard to organize and benchmark. For example, the main reported plots for EGFET pH sensors are the transfer and output characteristics of the nMOS at different pH values[33]— one issue with solely reporting these plots is the absence of the variation in time of the EGFET output. Moreover, rigorously determining an adequate response time to a steady state is difficult due to the constant drift of many pH sensing systems. For instance, the response time is defined by Wei et al. as the time needed for a sensor to reach 90% of its final value,[31] but, since all pH sensors experience a constant drift with time,[2,16,29,34–39] the final value is unclear.[40] Commonly investigated ISFET and EGFET pH sensing systems use a commercial reference electrode,[21,32,35,41–44] but the reference electrodes' properties and behavior are rarely reported, which leads to erroneously attributing their effect to the investigated sensing material. To give an example, solution-filled reference electrodes can have response times in the range of tens of seconds while gel-filled reference electrodes can have tens of minutes of stabilization time.[39,45,46] Furthermore, microfabricated versions of reference electrodes are more diverse and less stable; therefore, they require vital calibration before using in sensing systems.[47]

Another critical aspect is to assess the internal resistance (R_{in}) of pH systems' characterization instruments because of the high impedance of pH full cells. In general, for OCP measurements, the shunt resistance of the potentiometer used should be orders of magnitude greater than the resistance of the pH full cell. For quantification, glass sensing electrodes have membrane resistance of hundreds of MΩ.[48,49] Hence, the instrument measuring the potential between this electrode and the reference electrode should have an R_{in} in the hundreds of GΩ to TΩ range. Typical digital multimeters have R_{in} from 10 MΩ to 10 GΩ.[50] Today, semiconductor analyzers,[27,43,51] digital multimeters,[52,53] n-type and p-type commercial transistors,[26,40,53–55] instrumentation amplifiers,[53,55–57] electrometers,[12,58,59] electrochemical analyzers,[60] and pH meters[22,47,52] are used in pH sensing experiments, each with their own R_{in}. Different pH sensing devices have disparate full cell resistances due to differences in material resistivity (ρ) and sensing geometry, and thus the input resistance should scale accordingly. Dependence of measurement results on instruments' input resistance has been previously demonstrated for high impedance piezoelectric devices.[61] The emergence of wearable and implantable sensors makes the R_{in} and instrumentation requirements for portable pH sensing systems especially significant.[11,13,14,16,23,62–64] Hence, ρ of the sensing material, the overall resistance of the pH cell, and the resistance of the instrument used are important to fully characterize the viability of a pH sensing device. It is fairly possible that the better stability and response associated with some low ρ films[57,65] are attributed to an instrumentation issue. In other words, if the same instrument is used to characterize a pH cell with lower resistance, a relatively smaller portion of the cell current would pass in the instrument's resistance, leading to a smaller error.

Unlike traditional glass electrodes that are less prone to chemical reactions and fouling, pH sensing materials, such as ZnO, may react with or dissolve in testing solutions.[15,49,66,67] This issue is insignificant when calibration and testing times are kept short. However, when biomedical applications are targeted with long-term monitoring (approximately in hours), the surface modification of the sensing membrane becomes crucial. Reported pH sensing membranes with the response times in the order of few minutes[20,40,42,58,67–69] might experience surface modifications even during the calibration phase. This highlights the importance of assessing the pH sensing membrane's surface integrity during calibration and in the real application environment.

In this work, we show that intrinsic contributions of reference electrode and commercial transistor are not negligible. We further demonstrate the importance of time plots for EGFET setup. We also propose a convention for the determination of the current saturation value and for distinguishing the response from the onset of current drift. We, then, discuss the repeatability of pH measurements and its dependence on commonly used instruments, as well as precipitation fouling. Furthermore, we highlight the key tests and parameters necessary for an objective benchmarking of pH sensing systems for reproducible and reliable experimental reporting, which would lead to rapid progress in research and development of pH systems for biomedical applications.

2. Results and Discussion

2.1. Time Plots and Analysis of ZnO pH EGFET

2.1.1. Sensing Electrode and Experimental Setup

To study the importance of time plots for EGFET setup, we fabricate ZnO pH sensing electrodes. The fabrication steps of the extended gate sensing electrode and the EGFET experimental setup are shown in Figure S1 and Figure S2 in the Supporting Information, respectively (see the "Experimental Section" for the fabrication and setup details). The functional structure of the sensing electrode is 160 nm silicon dioxide (SiO_2)/10 nm chromium (Cr)/200 nm gold (Au)/320 nm ZnO. We use SiO_2 for electrical insulation, Cr for adhesion, and Au as the electrode. The electrode is connected to the gate terminal of a commercial n-type MOSFET (nMOSFET) (CD4007UB, Texas Instruments). Here, ZnO is the pH-sensitive membrane. The entire device structure is then encapsulated in polydimethylsiloxane (PDMS) with an exposed ZnO sensing area of 25 mm^2.

The ZnO film has $\rho > 160$ Ω cm, and polycrystalline structure with (002) and (103) preferred orientations, as seen in the scanning electron microscopy (SEM) image and grazing incidence X-ray diffraction (GIZRD) plots in **Figure 1**a and Figure 1b, respectively. Energy dispersive X-ray spectroscopy (EDAX) and X-ray photoelectron spectroscopy (XPS) show a consistent oxygen content in ZnO of ≈40% by atomic ratio at the surface and in the deep layers of the film (Figure 1c,d). ZnO inherently exhibits oxygen deficiency and it is an underlying
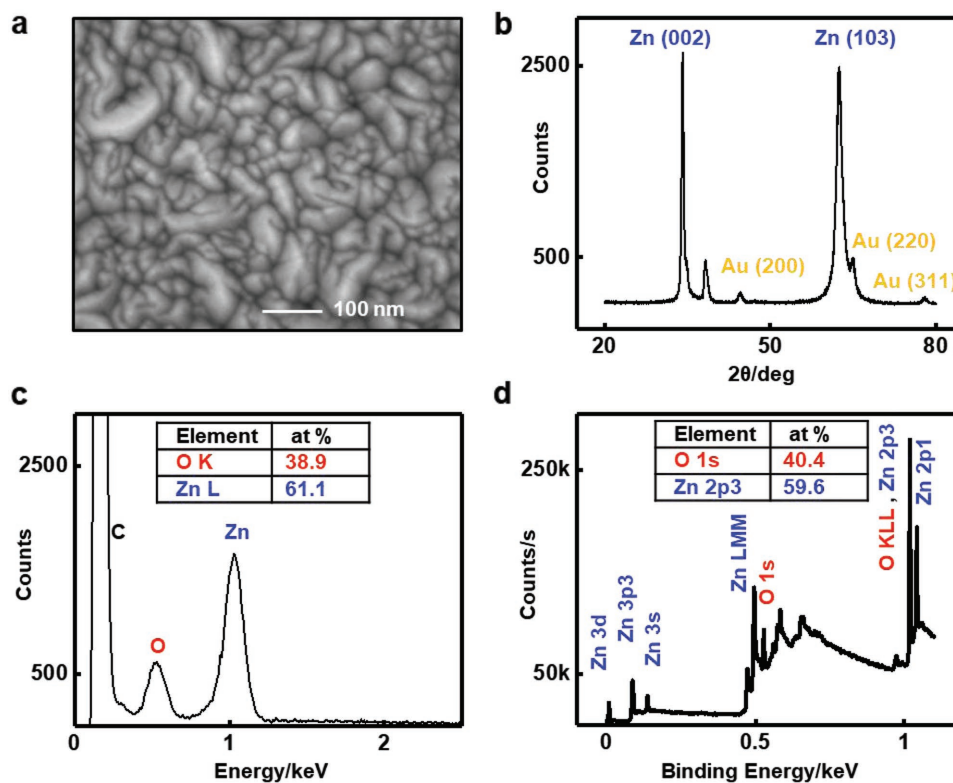
Figure 1. Properties of the sputtered ZnO film. a) Scanning electron microscope image shows grains ≈20 nm of the polycrystalline film. b) X-ray diffraction pattern of ZnO shows (002) and (103) preferred orientations. c) Energy dispersive analysis of ZnO shows volumetric zinc (Zn)-to-oxygen (O) ratio (at% is atomic percentage). d) X-ray photoelectron spectroscopy (XPS) survey confirms Zn-to-O ratio at the surface [the sample was argon (Ar) sputtered until the carbon peak disappeared to ensure the removal of organic contaminants].

cause of its behavior as n-type semiconductor.[70] Therefore, ≈40% O ratio is typical for sputtered ZnO thin films.[22]

2.1.2. Intrinsic Properties of pH System Components

For a controlled experiment where the concerned ZnO film is accurately studied, the intrinsic behavior of other components used in the system needs to be assessed. A semiconductor characterization system (Keithley 4200A-SCS, Tektronix), and shielded wires are used for all EGFET measurements in this section. The nMOSFET device has an R_{in} of ≈10^{12} Ω and an input capacitance of ≈10 pF.[71] All measurements are conducted at room temperature (20 °C) and under yellow light (≈580 nm). To assess the effect of ambient CO_2 on measurements, experiments using commercial Mettler Toledo pH and reference electrodes indicate that changes in solutions' pH due to exposure to air are negligible for the duration of our experiments (≈−0.002 pH) (details are shown in Figure S3a,b in the Supporting Information). The solutions' resistivity is ≈10 MΩ cm at direct current (DC) with 20% variation between pH 8 and pH 6. The leakage current into the gate of the transistor is ≈100 pA. This means that few millivolts will be always lost across the solution between reference and sensing electrodes, with a slightly higher loss for higher pH values. Since the loss is common to all solutions, it introduces a systemic error and does not affect sensitivity. Figure S3c (Supporting Information) shows the Bode plot for the buffer solutions.

First, we assess the stability of the nMOSFET with time in the saturation mode, i.e., drain to source voltage is greater or equal to effective gate voltage ($V_{eff} = V_{gs} - V_{th}$ and $V_{ds} \geq V_{eff}$, where V_{gs} is the gate-to-source voltage, V_{th} is the threshold voltage, and V_{ds} is the drain-to-source voltage). **Figure 2**a shows a consistent drift of the saturation current with a time of ≈18.6 µA h^{-1}. Reported sensitivities (S) for EGFET pH systems, extracted under similar saturation conditions, range between 15.8 and 79.9 µA pH^{-1}.[32,41,72–76] Noteworthy, the extraction of S values in A pH^{-1} from the output plot (I_{ds} vs V_{ds}) of the transistor in saturation mode ($V_{ds} \geq V_{eff}$) is not recommended because pH variation results in a shift in V_{gs} (i.e., pH ∝ V_{gs}) which modulates the drain-to-source current (I_{ds}). In saturation mode, the relation between I_{ds} and V_{gs} is quadratic ($I_{ds,saturation} \propto (V_{gs} - V_{th})^2$). Hence, a linear fit is more accurately represented by fitting a $\sqrt{I_{ds}}$ versus pH plot with S units in $A^{1/2}$ pH^{-1}. An example plot has been previously reported by Batista and Mulato in 2005, for EGFET's S in saturation,[33] and reported values in $A^{1/2}$ pH^{-1} lie between 0.26 and 1.36 µ$A^{1/2}$ pH^{-1}.[29,40,53,77,78] The process of getting a physically meaningful S in mV pH^{-1} from the EGFET I_{ds} versus V_{ds} output plot will be discussed with the relevant results.

Second, we measure the reference electrode stability in different solutions by connecting two silver (Ag)/silver chloride (AgCl) commercial electrodes (MW-2030 RE-6, BASi) with 3 M sodium chloride (NaCl) filling gel. One electrode is connected to the gate of the transistor; the other is connected to a constant
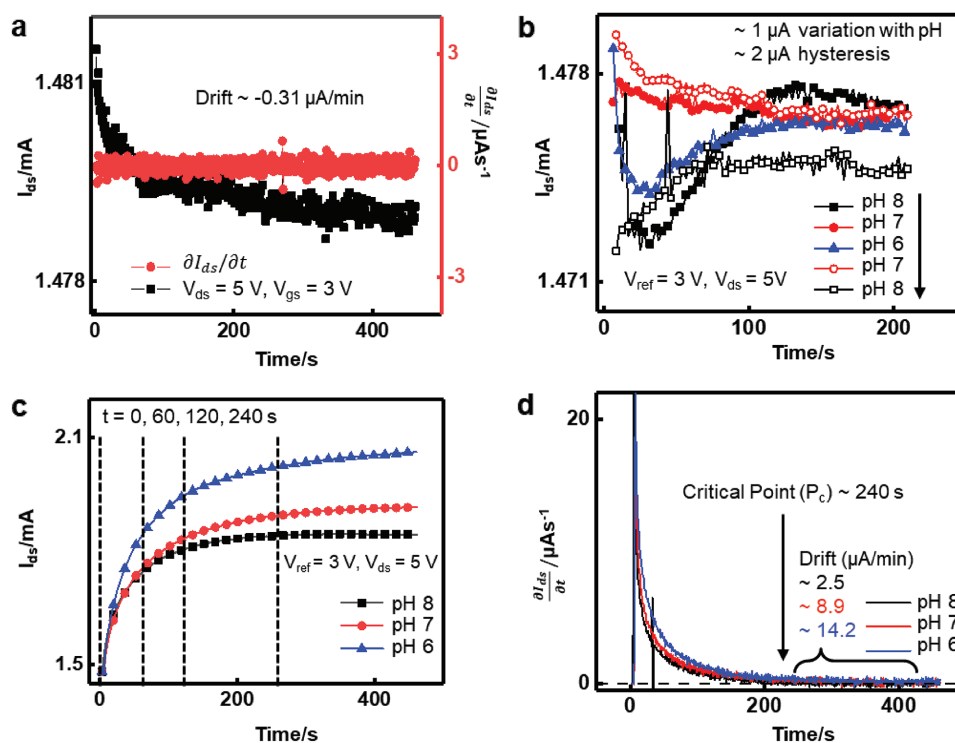
**ADVANCED
SCIENCE NEWS**

www.advancedsciencenews.com

**small
methods**

www.small-methods.com

Figure 2. Essential intrinsic and time plots for EGFET pH sensing setup displaying a) stability of the drain current of the used nMOS with time at saturation conditions (V_{ds} = 5 V, V_{gs} = 3 V), b) stability and variation in current response using two reference electrodes, c) actual drain current plot with time for ZnO sensing film versus Ag/AgCl reference electrode (the dash lines indicate different time instances to highlight the change in relative and absolute current values with time), and d) the first derivative of part (c) with time, highlighting the suggested placement of the critical point (P_c), and the estimated drift rates for solutions of different pH values.

3 V source to provide an offset voltage and ensure the transistor is kept in ON state (transistor $V_{th} \approx$ 1.5 V). The variation in I_{ds} due to reference electrode potential variations in time at different pH buffer solutions is shown in Figure 2b. All buffers (Inorganic Ventures, Inc.) consist of sodium hydroxide (NaOH) and potassium dihydrogenphosphate (KH$_2$PO$_4$) mixture with different concentrations (Table S1 in the Supporting Information provides the molar concentrations). Reasonable stability is achieved within ≈100 s, with variations of ≈1 µA with varying pH, and hysteresis within ≈2 µA.

2.2. ZnO EGFET and OCP Properties

Current flow variation with time at different pH values, for EGFET pH configuration, is crucial for determining how long the sensing and reference electrodes should remain in a tested solution. This, consequently, determines the time needed before the collection of correct output values and transfer plots. In our experiments, the sensing and reference electrodes are not conditioned with any special pretreatment, except rinsing in deionized (DI) water for a few seconds before and between the measurements. The results are shown in Figure 2c, with dotted lines highlighting variation in absolute and relative values at different time instances. Initially, there is a rapid change in current (I_{ds}) with time signifying the response regime. Subsequently, the slower change in I_{ds} with time indicates the drift regime. Observing the slopes of the three lines (pH 6, 7, and 8)

in the drift regime, it is evident that farther I_{ds} points in time have wider separation, i.e., the curves diverge with time. This is challenging since only one critical point (P_c) of I_{ds} should be extracted to plot against pH in the calibration plot. We define the P_c as the point at which the pH sensor response is complete, i.e., I_{ds} reached the full response value. P_c is then used to determine the response time as the time needed for I_{ds} to reach 90% of the full response. The full response is the difference between the I_{ds} at P_c and the initial I_{ds} value (I_{ds} at t = 0 s). In our case, I_{ds} at t = 0 s is fixed at ≈1.5 mA. This is the value that corresponds to I_{ds} when V_{gs} = 3 V and V_{ds} = 5 V, and is achieved through a resetting technique. Figure S2c (Supporting Information) illustrates the resetting technique, where the ZnO electrode is briefly connected to the reference electrode for resetting, then it is reconnected to the gate of the transistor (i.e., the measurement configuration). Hence, the starting point is fixed for all solutions and accumulated charges from previous measurements are dissipated. The drawback of this technique is that during the brief connection duration, current can flow through the low-resistance connection outside the pH cell, possibly shortening the useful life of the electrodes in the long run. To account for this drawback, a spare (i.e., control) sensor should be fabricated, and the control sensor undergoing this procedure should be excluded from use in the real application for providing quality control and longer lifespan of the electrode. Furthermore, the P_c is used in quantifying the drift from that time onward. One possible solution for identifying P_c is observing the first derivative of Figure 2c as depicted in

Figure 2d. P_c is the point at which a constant value is achieved, signifying a constant drift rate. For the reported ZnO film, P_c is ≈240 s, and corresponding drift values are 14.2, 8.9, and

2.5 µA min^{-1} for pH 6, 7, and 8, respectively (contribution from intrinsic transistor drift is −0.31 µA min^{-1}, Figure 2a). **Figure 3**a,b shows the corresponding output plots to the initial
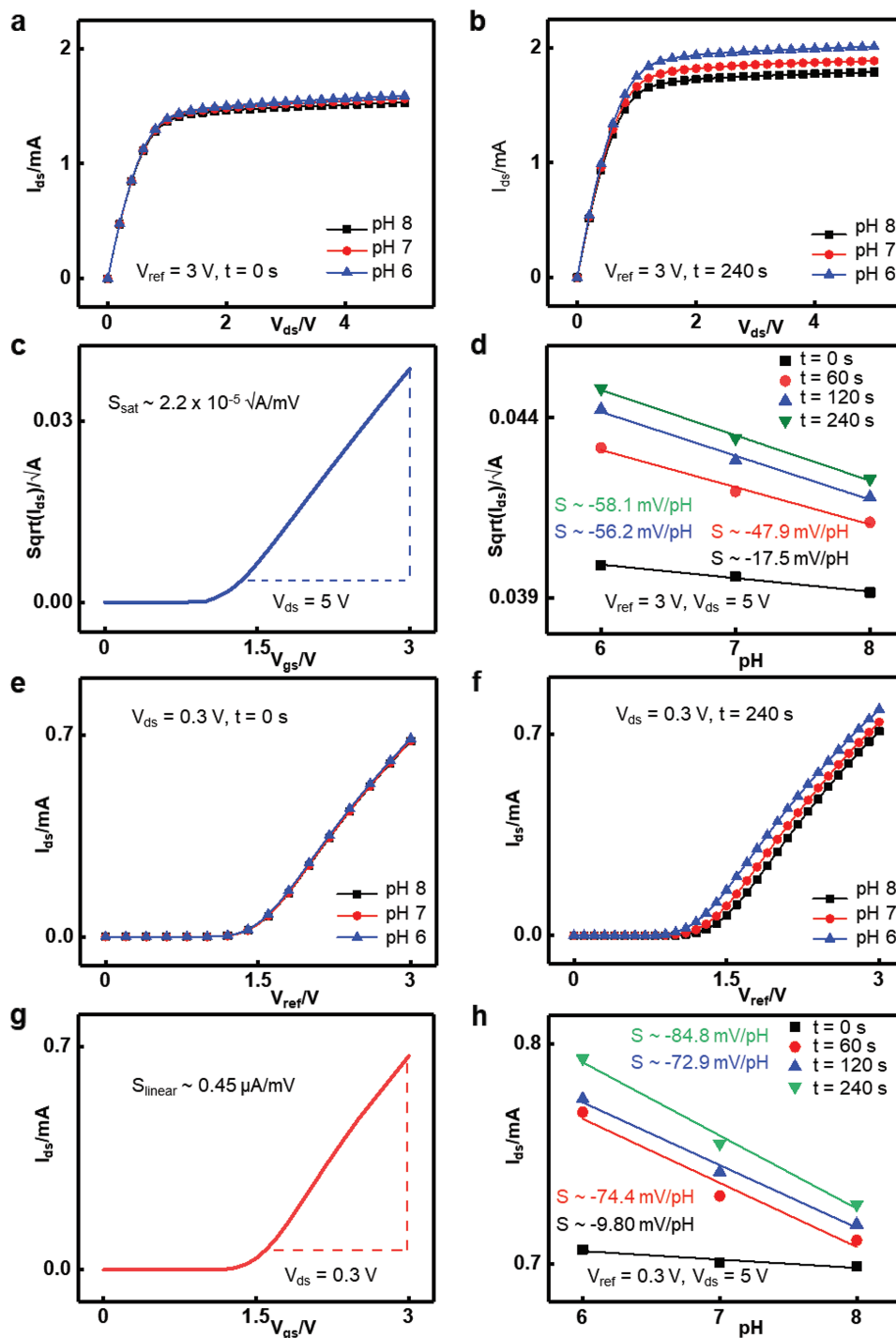

Figure 3. a–d) EGFET results analysis in the saturation mode ($V_{ds} \geq V_{gs} - V_{th}$) showing (a) EGFET output plot at $V_{ref} = 3$ V and time = 0 s, (b) output plot at $V_{ref} = 3$ V and time = 240 s, (c) plot for intrinsic $\sqrt{I_{ds}}$ versus V_{gs} of the nMOS transistor at $V_{ds} = 5$ V, and (d) $\sqrt{I_{ds}}$ versus pH of solution at different time instances and corresponding sensitivity values [sensitivity (S) = slope of the $\sqrt{I_{ds}}$ vs pH plot/slope of the $\sqrt{I_{ds}}$ vs V_{gs} plot (S_{sat})]. e–h) EGFET results analysis in the linear mode ($V_{ds} < V_{gs} - V_{th}$) showing e) transfer plot at $V_{ds} = 0.3$ V and time = 0 s, f) transfer plot at $V_{ds} = 0.3$ V and time = 240 s, g) plot for intrinsic I_{ds} versus V_{gs} of the nMOS transistor at $V_{ds} = 0.3$ V, and h) I_{ds} versus pH of solution at different time instances and corresponding sensitivity values (sensitivity (S) = slope of the I_{ds} vs pH plot/slope of the I_{ds} vs V_{gs} plot (S_{linear})).

ADVANCED
SCIENCE NEWS

www.advancedsciencenews.com

small
methods

www.small-methods.com

and final time instances from Figure 2c (all instances are given in Figure S4a–d in the Supporting Information). Evidently, the observed I_{ds} versus V_{ds}, at constant reference voltage (V_{ref}), significantly varies with the time at which the test is performed. To extract the S in saturation mode, we refer to the intrinsic transistor $\sqrt{I_{ds}}$ response to a V_{gs} sweep, at constant $V_{ds} = 5$ V (Figure 3c). The slope is then determined in $A^{1/2}$ mV^{-1}. A plot of $\sqrt{I_{ds}}$ versus pH value at $V_{ref} = 3$ and $V_{ds} = 5$ V is then constructed, and the slope is measured in $A^{1/2}$ pH^{-1} (Figure 3d). Together, the extracted slopes can be used to assess S in mV pH^{-1} (i.e., $A^{1/2}$ pH^{-1}/$A^{1/2}$ mV^{-1} = mV pH^{-1}). S in the saturation mode of the reported ZnO is −17.5, −47.9, −56.2, and −58.1 mV pH^{-1} at $t = 0$, 60, 120, and 240 s, respectively. Proper calibration relies on the line corresponding to the I_{ds} values at P_c (i.e., $t = 240$ s). Additionally, the integrity of the surface is visually monitored for modifications, which only become significant after prolonged hours of testing. The total time for all EGFET experiments using ZnO electrode is ≈35 min.

Similarly, the extraction method for S in linear regime needs to be revisited. Figure 3e,f provides similar plots for the ZnO EGFET in linear mode ($V_{ref} = 3$ V, $V_{ds} = 0.3$ V) and all instances are given in Figure S4e–h (Supporting Information). S extraction in linear mode is typically reported by choosing a fixed drain current value and identifying the intersection points with V_{ref} for different pH values.[29,40,41,53,77] Nonetheless, this method is not recommended for two reasons. First, V_{ref} is not directly related to the transistor's gate, compared to the current values which are actual currents flowing in the transistor. Second, the value of the constant current at which the horizontal line is drawn is arbitrary, which introduces significant errors based on the value of I_{ds} as well as when interpolating, if that was not an actually measured point in the system. On the other hand, a similar approach to the extraction in saturation mode would be a more reliable approach. The linear mode response of I_{ds} versus V_{gs} of the transistor is shown in Figure 3g.

Figure 3h displays the drain current values at $V_{ref} = 3$ V and $V_{ds} = 0.3$ V versus pH at different instances in time. The slopes of the latter two plots are used to extract S in mV pH^{-1}, varying from −9.8 to −84.8 mV pH^{-1} at $t = 0$ s and $t = 240$ s, respectively. These processes can be described by balancing the rates of nonequilibrium corrosion reactions to the different oxidation states at each electrode, and can therefore lead to non-Nernstian behavior (i.e., the −84.8 mV pH^{-1} super-Nernstian response could mean that one electron is transferred per 1.5 H$^+$ ions).[11,79–81] However, the results from saturation mode show S within the Nernstian limit for the same film. Hence, the inflated S values from linear mode might indicate an earlier equilibrium that significant drift would lead to a wider spread in the results, and a larger drift in linear versus saturation modes. The average hysteresis of the ZnO sensing EGFET is −62.2 µA (corresponding to ≈+0.5 pH units error, similar to typical reported values[82]) (Figure S5, Supporting Information). To overcome the hysteresis effect on calibration, all calibration points are collected from the same half-cycle from high to low pH values (i.e., unidirectional pH sweeps). Hysteresis is related to the recoverability of the sensing surface and the repeatability of the response. According to a recent study by Mackin et al., the sensor's response results from two adsorption mechanisms: one is reversible and the other is irreversible.[83] Accordingly, the

larger the irreversible component, the larger the hysteresis. The ZnO film dissolution rate in the pH 6–8 range is ≈20 nm per day (ZnO total thickness is 320 nm). Hence, film degradation is not a significant factor in the observed anomalies. Nonetheless, further analysis in OCP setup using a potentiostat (Reference 3000, Gamry Instruments), with ≈10^{11} ΩR_{in} in differential mode,[84] is also conducted for crossvalidation and comparing EGFET to traditional OCP results for the same device. For OCP measurements, the testing instrument R_{in} is critical while in the EGFET case, it is the MOSFET gate-to-source resistance that matters, as the sensing electrode only sees the isolated gate terminal of the circuit. The schematic of the OCP two-electrode setup, with the working and working sense electrodes connected to the ZnO sensing electrode, and the reference and counter electrodes connected to the Ag/AgCl reference electrode is presented in Figure S6a (Supporting Information). The OCP variation with time for different pH values and the corresponding first derivative plot are depicted in Figure S6b and Figure S6c (Supporting Information), respectively. A control experiment shows that the OCP setup with two Ag/AgCl reference electrodes exhibits ≈58 s response time and ≈1.88 mV h^{-1} (0.03 mV min^{-1}) drift. The results confirm the consistent behavior of the sensing electrode in a similar fashion as in the EGFET setup with $P_c ≈ 240$ s and $S = −62$ mV pH^{-1} at P_c, with higher S (32% increase) for delayed measurements due to the diverging drift (Figure S6d, Supporting Information). This emphasizes the importance of identifying P_c and using the values at that time for assessing sensitivity and other parameters. Worth mentioning, extracting the pH at point zero charge (pH$_{pzc}$) from the OCP versus pH plot at the point where OCP is zero is an invalid approximation because the OCP value is not necessarily equivalent to the surface potential at the ZnO/electrolyte interface. In fact, if the potential measured is due to a reaction at the electrode surface at equilibrium and not a junction potential, the OCP is independent of the surface potential. This arises because all the species in the electrical double layer (formed between the surface charges of the electrode and the attracted ions in the electrolyte) are in equilibrium with their bulk concentration. The OCP's dependence on pH can therefore is directly related to the electrochemical potential difference for electrons at each electrode, equivalent to representing the system as a galvanic cell. The electrochemical half-cell potential is given by the Nernst equation

$$\text{Half-cell reduction potential}: E_{red} = E_{red}^0 - \frac{RT}{zF} \ln \frac{a_{red}}{a_{ox}} \quad (1)$$

This can be converted to base-10 logarithm at 25 °C

$$E = E^0 - \frac{0.05916 \text{ V}}{z} \log_{10} \frac{a_{red}}{a_{ox}} \quad (2)$$

where E_{red} is the half-cell reduction potential, E_{red}^0 is the standard half-cell reduction potential, R is the universal gas constant, T is temperature in kelvin, z is the number of electrons transferred in the half-reaction, F is the Faraday constant, and a is the activity of the reduced or oxidized species. Applying Equation (2) to the reference electrode half-cell, the electrochemical reaction taking place is

**ADVANCED
SCIENCE NEWS**

www.advancedsciencenews.com

**small
methods**

www.small-methods.com

$$AgCl + e^- \rightleftarrows Ag + Cl^- \tag{3}$$

We get[85,86]

$$E_{AgCl} = E^0_{AgCl} - \frac{0.05916\text{ V}}{z}\log_{10}(a_{Cl-}) = 0.235 - 0.05916\log_{10}(a_{Cl-}) \tag{4}$$

The used AgCl reference electrode had an inner filling of 3 M NaCl, $z = 1$, and $a_{Cl-} = 3$ M, assuming the activity coefficient of one. This gives a half-cell reduction potential of 0.206 V. Ideally, a similar approach should be followed when calculating the half-cell potential of the ZnO sensing electrode. This is a challenging task because the exact reaction or reactions taking place on the ZnO surface are still unconfirmed to date. We can assume that an electrochemical reaction would lead to the production or consumption of protons, such as
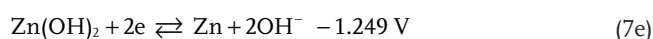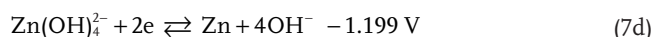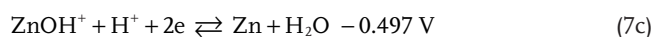
$$ZnO + 2H^+ + 2e^- \rightleftarrows Zn + H_2O \tag{5}$$

Applying Equation (2) conceptually to this reaction gives a half-cell potential that has a constant portion (E^0) and a pH-dependent component $\left(\frac{0.05916\text{ V}}{z}\log_{10}(a_{H+})\right)$. The actual measured full cell potential is the difference between the two half-cell reactions, given by
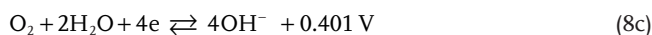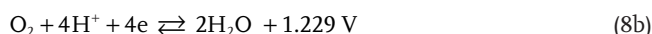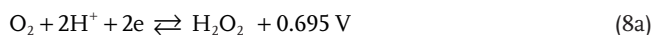
$$E_{cell} = E_{Sense} - E_{Ref} = E^0_{ZnO} - E^0_{AgCl} + \frac{0.05916\text{ V}}{z}\log_{10}(a_{H+})$$
$$+ \frac{0.05916\text{ V}}{z}\log_{10}(a_{Cl-}) = E^0_{ZnO} - \frac{0.05916\text{ V}}{z}\text{pH} - 0.206\text{ V} \tag{6}$$

However, the specific electrochemistry involved and number of electrons transferred is still unknown. The sensitivity at the P_c is 62.3 mV pH^{-1}, close to the Nernstian slope for a reaction involving one electron per proton reacted. The OCP of the pH full cell is 292.1, 218.9, 167.7 mV at pH 6, 7, 8, respectively. Substituting for the OCP value extracted from extrapolation at pH = 0 or $a_{H+} = 1$ M at standard state, $E_{cell} = 0.663$ V, in Equation (6), we get $E^0_{ZnO} = +0.869$ V. In basic solutions, the standard state at pH = 14 or $a_{OH-} = 1$ M extrapolates to $E_{cell} = -0.165$ V, and we get $E^0_{ZnO} = +0.041$ V.

The standard reduction potential of reactions involving Zn^{2+}, ZnO$_2^{2-}$, ZnOH$^+$, Zn(OH)$_4^{2-}$, Zn(OH)$_2$, and ZnO are given by (7),[87] with either pH = 0 or pH = 14 depending on whether H$^+$ or OH$^-$ participates in the reaction

$$Zn^{2+} + 2e \rightleftarrows Zn \quad -0.7618\text{ V} \tag{7a}$$

$$ZnO_2^{2-} + 2H_2O + 2e \rightleftarrows Zn + 4OH^- \quad -1.215\text{ V} \tag{7b}$$

$$ZnOH^+ + H^+ + 2e \rightleftarrows Zn + H_2O \quad -0.497\text{ V} \tag{7c}$$

$$Zn(OH)_4^{2-} + 2e \rightleftarrows Zn + 4OH^- \quad -1.199\text{ V} \tag{7d}$$

$$Zn(OH)_2 + 2e \rightleftarrows Zn + 2OH^- \quad -1.249\text{ V} \tag{7e}$$

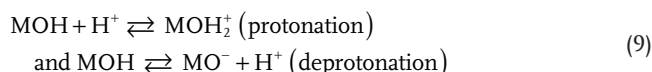$$ZnO + H_2O + 2e \rightleftarrows Zn + 2OH^- \quad -1.260\text{ V} \tag{7f}$$
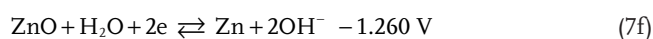
Hence, the positive standard reduction potential suggests either a different reaction or a mixed potential involving multiple simultaneous reactions. One possible reaction with positive standard reduction potential is oxygen evolution. However, the calculated value at the ZnO electrode does not map with a specific standard reduction potential value for possible oxygen evolution reactions ((13))[87]

$$O_2 + 2H^+ + 2e \rightleftarrows H_2O_2 \quad +0.695\text{ V} \tag{8a}$$

$$O_2 + 4H^+ + 4e \rightleftarrows 2H_2O \quad +1.229\text{ V} \tag{8b}$$

$$O_2 + 2H_2O + 4e \rightleftarrows 4OH^- \quad +0.401\text{ V} \tag{8c}$$

Therefore, it is likely that the latter hypothesis of a mixed potential is taking place, leading to corrosion and passivation of the ZnO surface. This might explain the observed continuous and constant drift that arises due to a continuously evolving surface, adding to the stability and repeatability challenges with ZnO. Table S2 (Supporting Information) represents calculated potential values at the sensing electrode from representative reported works of ZnO and iridium oxide (IrO$_x$) (another common pH sensing membrane for biomedical applications[11,88]). These values were extracted by extrapolating the reported voltage versus pH plots. The extracted value at pH of 0 (i.e., $a_{H+} = 1$ M) is then plugged into Equation (6) to estimate the reduction potential at the sensing electrode. For instance, the closer values of the calculated potential for IrO$_x$ electrodes to the standard reduction potentials of Ir redox reactions might explain the relatively more stable performance of IrO$_x$ versus ZnO membranes. The calculated potentials at the reported ZnO electrode vary significantly, and the magnitude of the potential is widely spread out from the expected standard reduction potentials involving the Zn ion. This topic is subject for further investigation, where the calculated potential values can predict the stability and repeatability of various pH sensing materials.

The above analysis assumes that no junction potentials are present in the system. As in the classical glass electrode, the measured potential difference may arise simply from a diffusion potential across the ZnO electrode among other possible reactions. For instance, i) diffusion of H$^+$ through the glass membrane, ii) facilitating the exchange of Na$^+$ and H$^+$ in solution by the glass membrane, and iii) generic binding site of weak dissociating groups of the glass membrane have all been proposed to explain the glass electrode's pH response.[59] Another common approach, relevant for the ISFET and EGFET setup, is to model the equilibrium surface charge density as a function of pH and, subsequently, relate the surface charge density to the measured potential via a model of the double layer. The model of the double layer involves the generic metal oxide chemical reactions shown in Equation (16)[82,89–91]

$$MOH + H^+ \rightleftarrows MOH_2^+ \text{ (protonation)}$$
$$\text{and } MOH \rightleftarrows MO^- + H^+ \text{ (deprotonation)} \tag{9}$$

where M represents the metal atom. This approach represents the system as a capacitance and is discussed with extraction of pH$_{pzc}$ in the Supporting Information.

2.3. Repeatability of pH Sensing Systems

Representative repeatability test for the ZnO electrode in OCP setup using Keithley 4200A SCS ($R_{in} \approx 10^{12}$ Ω[92,93] is presented in Figure S7 (Supporting Information); the inset shows the OCP values for the last 20 s from a full pH cycle (8→7→6→7→8). Measurements' starting point was fixed at zero by briefly connecting the two electrodes at the beginning of each measurement. Comparing Figure S7 and Figure S6b in the Supporting Information, minor variations exist given all variables (sensing electrode, reference electrode, buffers, and configuration) are the same except for the testing instrument. The Gamry Reference 3000 has an electrometer input impedance of ≈100 GΩ in parallel with a capacitance of ≈40 pF.[84] The Keithley 4200A SCS input capacitance can be neglected as the setup is calibrated with all wirings before the measurements to account for cable's impedance. In addition, guarded cables were used with the Keithley in OCP configuration, minimizing intrinsic sources of delay. Hence, the source of the variation rises from the higher input impedance of the Keithley and the possibly lower input capacitance.

Although different instruments, with comparable capabilities and results, might show minor deviations, different arrangements within the same instrument can exhibit severe distortions. To demonstrate the effect of instrumentation errors on pH measurement systems, a traditional glass electrode is used. A Mettler Toledo half-cell glass sensing electrode (InLab Mono, Mettler Toledo) is used with the BASi RE-6 Ag/AgCl reference electrode, and Keithley 4200A SCS is used for data acquisition in OCP configuration. The OCP setup involves sourcing zero current from the force terminal of a source measure unit (SMU) to the sensing electrode and connecting the sense low terminal of the same SMU to the reference electrode, while measuring the resulting voltage at the sensing electrode. Using a single SMU eliminates the errors that might be generated when two SMUs are competing for imposing an ideal zero current. **Figure 4**a,b shows the repeatability plots for the system in pH 6, 7, and 8. The same setup is used for multiple tests in pH 6, 7, and 8, while the current range is changed, which effectively changes the shunt resistance of the SMU. The variation of OCP results for the same system with varying input resistance of

the Keithley 4200A SCS is shown in **Figure 5**a–c. The significant role of the R_{in} is evident as results show different absolute values, separation with pH, and drift rates. These results are for a pH full-cell resistance of ≈600 MΩ (nominal resistance of glass sensing electrode plus the resistance of the reference electrode of a few kΩ). Hence, even a shunt resistance 15 times higher than the pH cell resistance (Figure 5c) has a significant effect on results, as confirmed by the different behavior in Figure 5d with >100 GΩ (≈10^{12} Ω nominal). Therefore, the ρ of pH sensing materials needs to be assessed before collecting measurements to ensure instrumentation effect is minimized.

Another issue affecting the repeatability of pH measurements is the surface modification of sensing films, especially when used for long-term measurements. Possibilities include dissolvability of the film and unwanted depositions from the test solutions.[94] Dissolution rates of pH sensing films, such as ZnO, have been previously studied.[53,95,96] On the other hand, unwanted depositions are hard to detect, and difficult to treat. Depending on the severity and rates of deposition, portions of the sensing area are rendered useless as they are insulated from contact with the electrolyte. Furthermore, during the long-term measurement, it is challenging to isolate the dependence of the results on the actual ion being sensed versus other ions that are adsorbed or deposited at the ZnO surface. Detailed discussion on fouling and selectivity is provided in the Supporting Information.

2.4. Recommendations on Benchmarking for pH Sensing Systems

Standardization and complete reporting are critical for the steady progress of research fields. The example from the semiconductor industry and its reliance on standard procedures and processes to sustain progress and development is worth replicating. For pH systems, standards are already in place for calibration buffers, glass electrodes, and pH meters but not for materials and configurations, such as the EGFET. We propose a list of recommended parameters to be reported for new pH materials/systems to facilitate accurate assessment and benchmarking. **Table 1** provides a summary of these
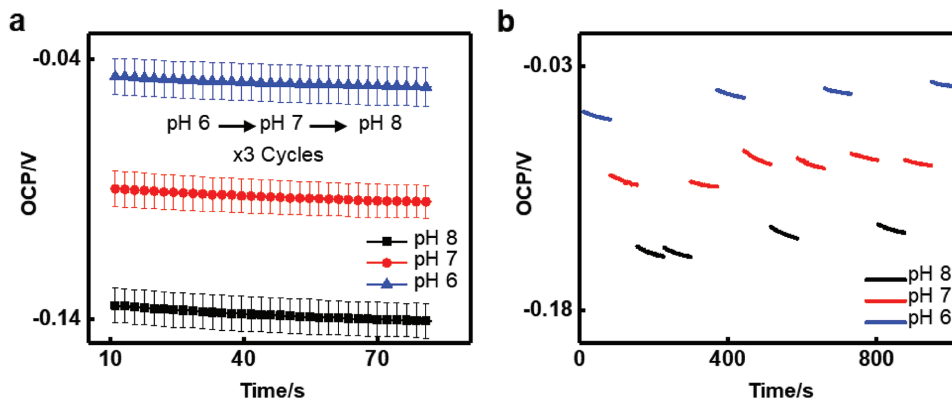

Figure 4. OCP results using Keithley 4200A SCS, Mettler Toledo glass sensing electrode, and BASi RE-6 reference electrode depicting a) OCP versus time plot for the last 1 min from three full pH 6,7 and 8 cycles, error bars represent standard deviation, and b) the unfolded results of OCP versus time sequence from the three cycles.
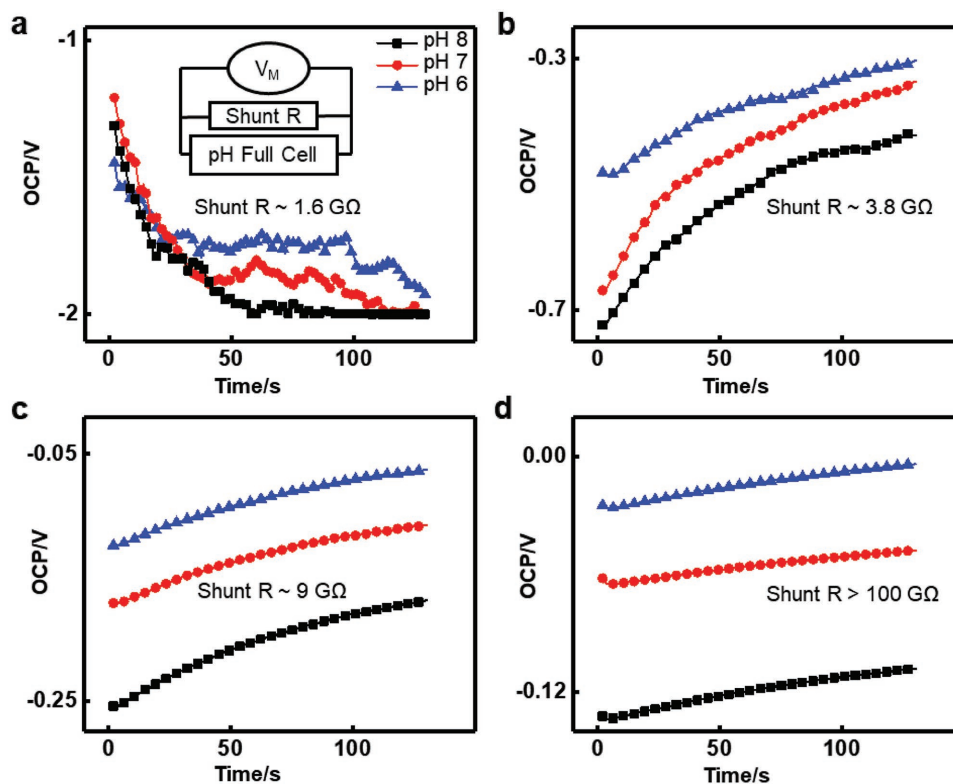
**ADVANCED
SCIENCE NEWS**

www.advancedsciencenews.com

**small
methods**

www.small-methods.com

Figure 5. OCP results with varying input resistances, using Keithley 4200A SCS, Mettler Toledo glass sensing electrode, and BASi RE-6 reference electrode for a) 100 µA range and $R \approx 1.6$ GΩ result, b) 10 µA range and $R \approx 3.8$ GΩ result, c) 1 µA range and $R \approx 9.0$ GΩ result, and d) 100 nA range and $R > 100$ GΩ result.

recommendations. A summary of results, comparing reported pH systems with our protocol, is provided in Table S3 (Supporting Information). Noteworthy, for EGFET examples in Table S3 (Supporting Information), the input resistance is

Table 1. Summary of recommendations for standardizing and benchmarking pH sensing materials and systems.

Category	Description	
Intrinsic characterization system properties	• Input resistance • Intrinsic time constant • Stability	
	Of all commercial components:	
	a) Characterization instrument b) Commercial transistor	c) Glass electrode d) Reference electrode
Intrinsic sensing film properties	• Composition • Crystallinity	• Thickness • Resistivity
Buffers and solutions properties	• Compositions • Concentrations	
Experimental techniques	• Conditioning surfaces before measurements • Intermittent cleaning between measurements	
Results	• Critical point (P_c) • Response time • Drift • Hysteresis • Sensitivity	• Selectivity • Repeatability • Fouling • pH range

dependent on the used transistor's gate-to-ground resistance which is $\approx 10^{12}$ Ω for the commonly reported CD4007UB transistor. The input resistance issue, in that case, is more relevant in other configurations that depend on the instrument's R_{in}, such as the studied OCP configuration. Nonetheless, it is essential to report the pH cell resistance, including the sensing film resistivity, because the ratio of pH full cell resistance to the instrument's (or transistor's) resistance is still important. Furthermore, selectivity column is eliminated because it is not reported in any of the listed works. Nonetheless, ZnO has been reported to exhibit satisfactory selectivity to Na^+ and K^+ at lower concentrations (1×10^{-6} M).[67] However, higher concentrations in the 10^{-3} M range require further selectivity studies that are still unavailable. Hence, reporting full compositions and concentrations of used solutions would enable extending the usefulness of the results for validating and correlating with future selectivity experiments. Similarly, when working with nonstoichiometric membranes like ZnO, reporting all essential film properties is mandatory. Otherwise, reproducing reported works would be unfeasible. For instance, the zinc-to-oxygen ratio is seldom reported, although, the different surface compositions would significantly impact the results. Reliable surface compositions can be achieved through XPS scans, as shown in Figure 1d and Figure S8d (Supporting Information). Adding the degree of tunability of ZnO makes the chance of achieving the targeted film challenging. Without knowing the composition of the reported films, the target for reproducing previous experimental results is undefined. Combining the discussed points

**ADVANCED
SCIENCE NEWS**

www.advancedsciencenews.com

**small
methods**

www.small-methods.com

with the lack of information about the structure of the reference electrode and its behavior, the intrinsic properties of commercial components, repeatability results, and the time sensitive parameters (i.e., response time and drift) limits the usefulness and impact of multiple reports. As a representative example, we summarize the ZnO EGFET experimental findings from this work by following the recommendations from our discussion (Table S3, Supporting Information).

3. Conclusion

The increasing demand for pH sensing in various applications, including biomedical field, necessitates continuous innovations in pH systems. Although great progress has been achieved, many reports do not contain key parameters for reproducibility and accurate benchmarking of materials. To this end, we experimentally demonstrated the importance of intrinsic contributions of commercial components and time plots for EGFET pH sensing systems, proposed a convention for determining a critical point for standardization of response time and drift values, and highlighted the dependence of the results on instruments' input resistance. These results and discussions collectively lead to the recommended pH system reporting. Our work is an important step toward addressing critical issues facing the standardization and benchmarking of pH sensing materials and systems. Valuable insights can be drawn from our suggested methods and be used for evaluating standard reduction potentials at the sensing electrode. Widespread use of our protocol would help to sustain continuous progress in the field of pH sensing.

4. Experimental Section

ZnO Electrode Fabrication: A silicon (100) wafer was used as a substrate. A 120 nm SiO_2 was then sputtered using the AJA 3-target sputtering system (AJA International Inc.) at room temperature. Denton E-beam Evaporator (Denton Vacuum, LLC) was used to evaporate 10 nm of Cr and 200 nm Au, without breaking the vacuum. A 320 nm ZnO film was deposited using an AJA 3-target sputtering system with 25 mm separation between the target and substrate, radio frequency (RF) power of 150 W, 15 sccm Ar, 7.5 sccm O_2 from an AJA ZnO target (99.99% purity, AJA International Inc.) at room temperature and 4 mT pressure. The base pressure before deposition was 5×10^{-7} T and the total ZnO sputtering time was 120 min. To make connections to the electrode, the ZnO was patterned using general purpose photoresist (SPR 220–3, MicroChem Corp.) to protect the sensing area, and buffered oxide etch (BOE 5:1 CMOS, Avantor Performance Materials Inc.) for 6 min. The exposed Au under the etched ZnO was connected via a wire and silver paste (C2130102D1, Sun Chemical Corporation). The whole structure was encapsulated in PDMS elastomer with a 10% curing agent (Sylgard 184, MilliporeSigma), cured at 60 °C for 2 h with a 25 mm^2 opening area for the ZnO sensing. Figure S1 (Supporting Information) shows the fabrication process of the ZnO electrode.

ZnO Electrode Characterization: The ρ value of the ZnO film (>160 Ω cm) was measured from a similar ZnO film on glass substrate, using a four-point Probe system (CDE-ResMap, Creative Design Engineering, Inc.). The crystallinity of the ZnO film was measured using a grazing incidence X-ray diffraction (GIXRD) scan (Smartlab Multipurpose Diffractometer, Rigaku Corporation) with an incident angle of 0.5°, and the Zn:O ratio at the surface and in bulk was extracted from PHI VersaProbe II XPS (Physical Electronics, Inc.) and Zeiss Ultra Plus EDAx (Zeiss International),

respectively. Figure S2a (Supporting Information) illustrates the experimental EGFET setup used to characterize the pH sensing properties of the ZnO electrode. The schematic and connection pins to the nMOS transistor in CD4007UB package (Texas Instruments) are depicted in Figure S2b (Supporting Information). A BASi RE-6 Ag/AgCl reference electrode with gel type 3 M NaCl internal solution was utilized. For I_{ds} versus time plots, the reference electrode was biased at 3 V, drain voltage was biased at 5 V, and the drain current was monitored with time in different pH buffers using a Keithely 4200A SCS. The input resistances of the Keithley 4200A SCS and the nMOS transistor were >1 TΩ, and the sampling time was 1 s. The full pH cell resistance was >30 GΩ. The drain and reference voltages were swept in 100 mV increments for output and transfer plots, respectively. The compositions and concentrations of the used buffer solutions 6, 7, and 8 are provided in Table S1 (Supporting Information).

Glass and Reference Electrodes: For the instrumentation input resistance experiments, a half-cell pH sensing electrode (InLab Mono glass sensing electrode, Mettler Toledo) with <600 MΩ membrane resistance, pH_{pzc} of 7 ($\pm$0.25), response time of 20 s, and sensitivity of >57.8 mV pH^{-1} was used. A reference electrode (InLab Reference Electrode, Mettler Toledo) of diaphragm resistance 5.5 kΩ, with internal filling 3 M potassium chloride (KCl) solution was used.

Supporting Information

Supporting Information is available from the Wiley Online Library or from the author.

Conflict of Interest

The authors declare no conflict of interest.

[1] M. S. Lesney, *Today's Chem. Work* **2003**, 47.
[2] P. Kurzweil, *Sensors* **2009**, 9, 4955.
[3] A. A. Belyustin, *J. Solid State Electrochem.* **2011**, 15, 47.
[4] A. J. Bard, L. R. Faulkner, *Electrochemical Methods : Fundamentals and Applications*, John Wiley & Sons, New York **2001**.
[5] A. K. Convington, R. G. Bates, R. A. Durst, *Pure Appl. Chem.* **1985**, 57, 531.
[6] P. Bergveld, *IEEE Trans. Biomed. Eng.* **1970**, BME-17, 70.
[7] D. E. Yates, S. Levine, T. W. Healy, *J. Chem. Soc., Faraday Trans. 1* **1974**, 70, 1807.
[8] J. van der Spiegel, I. Lauks, P. Chan, D. Babic, *Sens. Actuators* **1983**, 4, 291.
[9] S. M. Al-Hilli, R. T. Al-Mofarji, M. Willander, *Appl. Phys. Lett.* **2006**, 89, 173119.
[10] P. D. Batista, M. Mulato, *J. Mater. Sci.* **2010**, 45, 5478.
[11] H. J. Chung, M. S. Sulkin, J. S. Kim, C. Goudeseune, H. Y. Chao, J. W. Song, S. Y. Yang, Y. Y. Hsu, R. Ghaffari, I. R. Efimov, J. A. Rogers, *Adv. Healthcare Mater.* **2014**, 3, 59.
[12] P. Y. Chen, L. Te Yin, T. H. Cho, *Life Sci. J.* **2014**, 11, 871.
[13] T. Guinovart, G. Valdés-Ramírez, J. R. Windmiller, F. J. Andrade, J. Wang, *Electroanalysis* **2014**, 26, 1345.
[14] P. Fanzio, C.-T. Chang, M. Skolimowski, S. Tanzi, L. Sasso, *Sensors* **2017**, 17, 1169.
[15] R. Sha, K. Komori, S. Badhulika, *IEEE Sens. J.* **2017**, 17, 5038.
[16] H. Y. Y. Nyein, W. Gao, Z. Shahpar, S. Emaminejad, S. Challa, K. Chen, H. M. Fahad, L. C. Tai, H. Ota, R. W. Davis, A. Javey, *ACS Nano* **2016**, 10, 7216.
[17] O. Korostynska, K. Arshak, E. Gill, A. Arshak, *Sensors* **2007**, 7, 3027.
[18] L. Chen, L. He, F. Ma, W. Liu, Y. Wang, M. A. Silver, L. Chen, L. Zhu, D. Gui, J. Diwu, Z. Chai, S. Wang, *ACS Appl. Mater. Interfaces* **2018**, 10, 15364.
[19] B. Saravanakumar, S. Soyoon, S.-J. Kim, *ACS Appl. Mater. Interfaces* **2014**, 6, 13716.
[20] A. Fulati, S. M. Usman Ali, M. Riaz, G. Amin, O. Nur, M. Willander, *Sensors* **2009**, 9, 8911.
[21] L. Maiolo, S. Mirabella, F. Maita, A. Alberti, A. Minotti, V. Strano, A. Pecora, Y. Shacham-Diamand, G. Fortunato, *Appl. Phys. Lett.* **2014**, 105, 093501.
[22] G. K. Mani, M. Morohoshi, Y. Yasoda, S. Yokoyama, H. Kimura, K. Tsuchiya, *ACS Appl. Mater. Interfaces* **2017**, 9, 5193.
[23] S. Nakata, T. Arie, S. Akita, K. Takei, *ACS Sens.* **2017**, 2, 443.
[24] R. Rahimi, M. Ochoa, T. Parupudi, X. Zhao, I. K. Yazdi, M. R. Dokmeci, A. Tamayol, A. Khademhosseini, B. Ziaie, *Sens. Actuators, B* **2016**, 229, 609.
[25] M. Caldara, C. Colleoni, M. Galizzi, E. Guido, V. Re, G. Rosace, A. Vitali, in *2012 IEEE Sensors*, IEEE, Taipei, Taiwan **2012**, pp. 1–4.
[26] P. D. Batista, M. Mulato, *Appl. Phys. Lett.* **2005**, 87, 143508.
[27] G. M. Ali, *J. Electron. Mater.* **2017**, 46, 713.
[28] C. T. Lee, Y. S. Chiu, L. R. Lou, S. C. Ho, C. Te Chuang, *IEEE Sens. J.* **2014**, 14, 490.
[29] J. L. Wang, P. Y. Yang, T. Y. Hsieh, P. C. Juan, *Jpn. J. Appl. Phys.* **2016**, 55, 01AE16.
[30] Y. S. Chiu, C. Y. Tseng, C. T. Lee, *IEEE Sens. J.* **2012**, 12, 930.
[31] A. Wei, L. Pan, W. Huang, *Mater. Sci. Eng., B* **2011**, 176, 1409.
[32] S.-P. Chang, C.-W. Li, K.-J. Chen, S.-J. Chang, C.-L. Hsu, T.-J. Hsueh, H.-T. Hsueh, *Sci. Adv. Mater.* **2012**, 4, 1174.
[33] P. D. Batista, M. Mulato, *Appl. Phys. Lett.* **2005**, 87, 1.
[34] Q. Zhang, W. Liu, C. Sun, H. Zhang, W. Pang, D. Zhang, X. Duan, *Nanotechnology* **2015**, 26, 1.
[35] J. C. Chou, Y. F. Wang, *Sens. Actuators, B* **2002**, 86, 58.
[36] W. Lonsdale, M. Wajrak, K. Alameh, *Sensors* **2017**, 17, 2036.
[37] J. C. Chou, S. J. Yan, Y. H. Liao, C. H. Lai, J. S. Chen, H. Y. Chen, T. W. Tseng, J. T. Wu, *IEEE Sens. J.* **2017**, 18, 605.
[38] P.-Y. Yang, J.-L. Wang, P.-C. Chiu, J.-C. Chou, C.-W. Chen, H.-H. Li, H.-C. Cheng, *IEEE Electron Device Lett.* **2011**, 32, 1603.
[39] U. Guth, F. Gerlach, M. Decker, W. Oelßner, W. Vonau, *J. Solid State Electrochem.* **2009**, 13, 27.
[40] E. J. Guidelli, E. M. Guerra, M. Mulato, *ECS J. Solid State Sci. Technol.* **2012**, 1, N39.
[41] J.-Y. Li, S.-P. Chang, S.-J. Chang, T.-Y. Tsai, *ECS Solid State Lett.* **2014**, 3, P123.
[42] K. B. Parizi, X. Xu, A. Pal, X. Hu, H. S. Philip Wong, *Sci. Rep.* **2017**, 7, 1.
[43] G. M. Ali, H. D. Ra'ad, A. A. Abdullateef, in *Technological Advances in Electrical, Electronics and Computer Engineering (TAEECE), 2015 Third Int. Conf. on*, IEEE, Beirut, Lebanon **2015**, pp. 234–238.
[44] Y. S. Chiu, C. T. Lee, L. R. Lou, S. C. Ho, C. Te Chuang, *Sens. Actuators, B* **2013**, 188, 944.
[45] Mettler Toledo, *The Right Electrolyte* **2012**, pp. 1–3.
[46] P. Tallgren, S. Vanhatalo, K. Kaila, J. Voipio, *Clin. Neurophysiol.* **2005**, 116, 799.
[47] M. Waleed Shinwari, D. Zhitomirsky, I. A. Deen, P. R. Selvaganapathy, M. Jamal Deen, D. Landheer, *Sensors* **2010**, 10, 1679.
[48] Mettler Toledo, *InLab Sensors* **2017**.
[49] Rosemount Analytical, *The Theory of pH Measurement* **2010**.
[50] Keysight Technologies, *Digital Multimeters* **2017**.
[51] J. Chiang, S. Tsai, in *Nanoelectronics Conf. (INEC), 2013 IEEE 5th Int.*, IEEE, Singapore, Singapore **2013**, pp. 502–504.
[52] P. Salvo, N. Calisi, B. Melai, V. Dini, C. Paoletti, T. Lomonaco, A. Pucci, F. Di Francesco, A. Piaggesi, M. Romanelli, *Int. J. Nanomed.* **2017**, 12, 949.
[53] N. Al-Hardan, M. Abdul Hamid, N. Ahmed, A. Jalar, R. Shamsudin, N. Othman, L. Kar Keng, W. Chiu, H. Al-Rawi, *Sensors* **2016**, 16, 839.
[54] B.-R. Huang, J.-C. Lin, Y.-K. Yang, *J. Electrochem. Soc.* **2013**, 160, B78.
[55] P. D. Batista, *Meas. Sci. Technol.* **2014**, 25, 027001.
[56] L. Te Yin, J. C. Chou, W. Y. Chung, T. P. Sun, S. K. Hsiung, *Mater. Chem. Phys.* **2001**, 70, 12.
[57] J. L. Lin, Y. M. Chu, S. H. Hsiao, Y. L. Chin, T. P. Sun, *Jpn. J. Appl. Phys., Part 1* **2006**, 45, 7999.
[58] C. Ratanapornacharoen, M. Tabata, Y. Kitasako, M. Ikeda, T. Goda, A. Matsumoto, J. Tagami, Y. Miyahara, *Anal. Chem.* **2018**, 90, 4925.
[59] D. J. Graham, B. Jaselskis, C. E. Moore, *J. Chem. Educ.* **2013**, 90, 345.
[60] J. Park, Y. Jeong, I. Park, in *Micro Electro Mechanical Systems (MEMS), 2017 IEEE 30th Int. Conf. on*, IEEE, Las Vegas, NV, USA **2017**, pp. 494–497.
[61] Y. Su, C. Dagdeviren, R. Li, *Adv. Funct. Mater.* **2015**, 25, 5320.
[62] K. B. Mirza, C. Zuliani, B. Hou, F. S. Ng, N. S. Peters, C. Toumazou, in *Engineering in Medicine and Biology Society (EMBC), 2017 39th Annual Int. Conf. of the IEEE*, IEEE, Seogwipo, South Korea **2017**, pp. 189–192.
[63] M. Punjiya, H. Rezaei, M. A. Zeeshan, S. Sonkusale, in *Solid-State Sensors, Actuators and Microsystems (TRANSDUCERS), 2017 19th Int. Conf. on*, IEEE, Kaohsiung, Taiwan **2017**, pp. 1700–1702.
[64] R. Aparecido, S. Nascimento, M. Mulato, U. F. De Lavras, *Mater. Res.* **2017**, 20, 1369.
[65] C. E. Lue, I. S. Wang, C. H. Huang, Y. T. Shiao, H. C. Wang, C. M. Yang, S. H. Hsu, C. Y. Chang, W. Wang, C. S. Lai, *Microelectron. Reliab.* **2012**, 52, 1651.
[66] N. Izyumskaya, A. Tahira, Z. H. Ibupoto, N. Lewinski, V. Avrutin, Ü. Özgür, E. Topsakal, M. Willander, H. Morkoç, *ECS J. Solid State Sci. Technol.* **2017**, 6, Q84.
[67] M. Willander, S. Al-Hilli, *Methods Mol. Biol.* **2009**, 544, 187.
[68] H. J. Jang, J. G. Gu, W. J. Cho, *Sens. Actuators, B* **2013**, 181, 880.
[69] J. C. Fernandes, R. A. S. Nascimento, M. Mulato, *Mater. Res.* **2016**, 19, 267.
[70] A. M. C. Ng, X. Y. Chen, A. B. Djuri, *Prog. Quantum Electron.* **2010**, 34, 191.

[71] Instruments Texas, *CMOS Dual Complementary Pair Plus Inverter* **2003**.

[72] S. P. Chang, T. H. Yang, *Int. J. Electrochem. Sci.* **2012**, *7*, 5020.

[73] H. Oh, K. J. Lee, J. Baek, S. S. Yang, K. Lee, *Microelectron. Eng.* **2013**, *111*, 154.

[74] S. X. Chen, S. P. Chang, S. J. Chang, *Dig. J. Nanomater. Biostruct.* **2014**, *9*, 1505.

[75] P. C. Yao, M. C. Lee, J. L. Chiang, in *Computer, Consumer and Control (IS3C), 2014 Int. Symp. on*, IEEE, Taichung, Taiwan **2014**, pp. 577–580.

[76] P. Y. Lee, S. P. Chang, P. J. Kuo, E. H. Hsu, S. J. Chang, S. C. Shei, *Int. J. Electrochem. Sci.* **2013**, *8*, 3866.

[77] P. Van Thanh, L. T. Q. Nhu, H. H. Mai, N. V. Tuyen, S. C. Doanh, N. C. Viet, D. T. Kien, *J. Electron. Mater.* **2017**, *46*, 3732.

[78] H. S. Rasheed, N. M. Ahmed, M. Z. Matjafri, *Mater. Sci. Semicond. Process.* **2018**, *74*, 51.

[79] I. Valsiunas, K. Juodkazis, *Electroanalysis* **2005**, *17*, 947.

[80] G. M. Silva, S. G. Lemos, L. A. Pocrifka, P. D. Marreto, A. V Rosario, E. C. Pereira, *Anal. Chim. Acta* **2008**, *616*, 36.

[81] L. Burke, D. Whelan, *J. Electroanal. Chem. Interfacial Electrochem.* **1984**, *162*, 121.

[82] F. A. Sabah, N. M. Ahmed, Z. Hassan, M. A. Almessiere, *Mater. Sci. Semicond. Process.* **2017**, *71*, 217.

[83] C. Mackin, V. Schroeder, A. Zurutuza, C. Su, J. Kong, T. M. Swager, T. Palacios, *ACS Appl. Mater. Interfaces* **2018**, *10*, 16169.

[84] Gamry Instruments, *Reference 3000. Potentiostat/Galvanostat/ZRA Operator's Manual* **2017**.

[85] S. M. Al-Hilli, R. T. Al-Mofarji, P. Klason, M. Willander, N. Gutman, A. Sa'Ar, *J. Appl. Phys.* **2008**, *103*, 014302.

[86] *CRC Handbook of Chemistry and Physics* (Ed: D. D. Lide), 87 ed., CRC Press, Boca Raton, FL, USA **2005**, p. 1.

[87] P. Vanýsek, in *CRC Handbook of Chemistry and Physics* (Ed: W. M. Haynes), CRC Press, Boca Raton, FL, USA **1998**, pp. 20–29.

[88] E. Prats-Alfonso, L. Abad, N. Casañ-Pastor, J. Gonzalo-Ruiz, E. Baldrich, *Biosens. Bioelectron.* **2013**, *39*, 163.

[89] J. C. Chou, Y. S. Li, J. L. Chiang, *Sens. Actuators, B* **2000**, *71*, 73.

[90] S. Zaman, M. H. Asif, A. Zainelabdin, G. Amin, O. Nur, M. Willander, *J. Electroanal. Chem.* **2011**, *662*, 421.

[91] F. A. Sabah, N. M. Ahmed, Z. Hassan, M. Abdullah Almessiere, *Mater. Sci. Semicond. Process.* **2017**, *63*, 269.

[92] Keithley Instruments, *Optimizing Low Current Measurements with the Model 4200-SCS Semiconductor Characterization System* **2008**.

[93] Keithley Instruments, *Semiconductor Characterization System Technical Data* **2011**.

[94] S. Kakooei, C. Ismail, B. Ari-Wahjoedi, *Int. J. Mater. Sci. Innovations* **2013**, *1*, 62.

[95] K. Meziane, A. El Hichou, A. El Hamidi, M. Mansori, A. Liba, A. Almaggoussi, *Superlattices Microstruct.* **2016**, *93*, 297.

[96] C. Dagdeviren, S. W. Hwang, Y. Su, S. Kim, H. Cheng, O. Gur, R. Haney, F. G. Omenetto, Y. Huang, J. A. Rogers, *Small* **2013**, *9*, 3398.